The Roles of Tyr(CD1) and Trp(G8) in *Mycobacterium tuberculosis* Truncated Hemoglobin O in Ligand Binding and on the Heme Distal Site Architecture[†,‡]

Hugues Ouellet,[§,||] Mario Milani,[⊥] Marie LaBarre,[§] Martino Bolognesi,[⊥] Manon Couture,[§] and Michel Guertin*[,§]

Department of Pharmaceutical Chemistry, University of California, San Francisco, California 94143-0446, Department of Biomolecular Sciences and Biotechnology and CNR-INFM, University of Milano, Via Celoria, 26, I-20133 Milano, Italy, and Department of Biochemistry and Microbiology, Laval University, Quebec, Canada, G1K 7P4

Received May 25, 2007; Revised Manuscript Received August 6, 2007

ABSTRACT: The crystal structure of the cyano-met form of *Mt*-trHbO revealed two unusual distal residues Y(CD1) and W(G8) forming a hydrogen-bond network with the heme-bound ligand [Milani, M., et al. (2003) *Proc. Natl. Acad. Sci. U.S.A. 100*, 5766−5771]. W(G8) is an invariant residue in group II and group III trHbs and has no counterpart in other globins. A previous study reported that changing Y(CD1) for a Phe causes a significant increase in the O_2 combination rate, but almost no change in the O_2 dissociation rate [Ouellet, H., et al. (2003) *Biochemistry 42*, 5764−5774]. Here we investigated the role of the W(G8) in ligand binding by using resonance Raman spectroscopy, stopped-flow spectrophotometry, and X-ray crystallography. For this purpose, W(G8) was changed, by site-directed mutagenesis, to a Phe in both the wild-type protein and the mutant Y(CD1)F to create the single mutant W(G8)F and the double mutant Y(CD1)F/W(G8)F, respectively. Resonance Raman results suggest that W(G8) interacts with the heme-bound O_2 and CO, as evidenced by the increase of the Fe−O_2 stretching mode from 559 to 564 cm^{-1} and by the lower frequency of the Fe−CO stretching modes (514 and 497 cm^{-1}) compared to that of the wild-type protein. Mutation of W(G8) to Phe indicates that this residue controls ligand binding, as evidenced by a dramatic increase of the combination rates of both O_2 and CO. Also, the rate of O_2 dissociation showed a 90−1000-fold increase in the W(G8)F and Y(CD1)F/W(G8)F mutants, that is in sharp contrast with the values obtained for the other distal mutants Y(B10)F and Y(CD1)F [Ouellet, H., et al. (2003) *Biochemistry 42*, 5764−5774]. Taken together, these data indicate a pivotal role for the W(G8) residue in O_2 binding and stabilization.

In *Mycobacterium tuberculosis* the *glbO* gene encodes the truncated hemoglobin *Mt*-trHbO.[1] The function of *Mt*-trHbO is unknown. Its very high affinity for O_2 (nanomolar range) due to a very slow release of O_2 (0.004 s^{-1}) makes it unlikely that its function is the delivery of O_2. In addition, the slow oxidation of NO by oxygenated *Mt*-trHbO (0.6 μM^{-1} s^{-1}) in comparison to that observed for *Mt*-trHbN-O_2 (745 μM^{-1} s^{-1}) and Mb-O_2 (35−45 μM^{-1} s^{-1}) also makes a NO detoxification an unlikely role for *Mt*-trHbO (*2*−*5*). A previous study suggests that *Mt*-trHbO may carry out rapid oxidation/reduction reactions with H_2O_2, and possibly O_2 as the oxidant (*6*).

Mt-trHbO belongs to group II trHbs. Four branches, represented by the Actinobacteria, Proteobacteria, Firmicutes (bacteria), and plants, form group II trHbs (*7*−*9*). The most distinctive feature characterizing trHbs from each branch is the presence in the heme distal site cavity of a specific and conserved array of polar residues at globin topological sites B10, CD1, E7, E11, and G8 (*7*, *9*). To date, two cyano-met group II crystal structures have been reported, that of *M. tuberculosis* (*Mt*-trHbO) (Actinobacterium) and that of *Bacillus subtilis* trHb (*Bs*-trHbO) (Firmicute) (*1*, *10*). Additionally, the crystal structures of the ferric acetate derivative of group II trHb from *Thermobifida fusca* (*Tf*-trHbO) and *Geobacillus stearothermophilus* (*Gs*-trHbO) have been reported (*11*, *12*). In *Mt*-trHbO the heme bound cyanide is stabilized by a strong hydrogen bond (2.8 Å) connecting the ligand to Y(CD1) (with a weaker hydrogen bond, 3.3 Å, to W(G8)) while in *Bs*-trHbO (displaying Phe at the CD1 site) the heme-bound ligand is stabilized by residue Y(B10) (hydrogen bond of 2.6 Å). Interestingly, even though both proteins display a tyrosine at the B10 site, the crystal structures indicate that only in *Bs*-trHbO does Y(B10) stabilize the bound cyanide. In *Mt*-trHbO an additional

[†] This work was supported by the National Sciences and Engineering Research Council (NSERC) Grant 46306-01 (2005-2010) to M.G. M.B. is grateful to CIMAINA (Milano, Italy) for continuous support. Part of this study was supported by the Italian Ministry for University and Scientific Research FIRB Project "Biologia Strutturale" to M.B., Contract RBLA03B3KC. M.M. is recipient of a postdoctoral fellowship under NIH Contract 1-R01-AI052258. M.C. is supported by the NSERC Grant 250073 and the Fonds Québécois de la Recherche sur la Nature et les Technologies (FQRNT) Grant 78927.

[‡] The PDB accession code for the cyano-met structure is 2QRW.

* Corresponding author: Department of Biochemistry and Microbiology, Pavillon Marchand, Room 3145. Tel: 418-656-2131 ext 5581. Fax: 418-656-7176. E-mail: mguertin@bcm.ulaval.ca.

[§] Laval University.

[||] University of California.

[⊥] University of Milano.

[1] Abbreviations: trHb, truncated hemoglobin; *Mt*-trHbO, *Mycobacterium tuberculosis* truncated hemoglobin O; *Bs*-trHbO, *Bacillus subtilis* truncated hemoglobin O; *Tf*-trHbO, *Thermobifida fusca* truncated hemoglobin O*; Gs*-trHbO, *Geobacillus stearothermophilus* truncated hemoglobin O; GdmCl, guanidium chloride; *Cj*-trHbP, *Campylobacter jejuni* truncated hemoglobin P. Residues of *Mt*-trHbO have been identified by their one-letter codes and by their topological position within the globin fold.

10.1021/bi7010288 CCC: $37.00
Published on Web 09/22/2007

Table 1: Frequencies of the Vibrational Modes of the Deoxy, O_2, and CO Derivatives of *Mt*-trHbO and Its Mutants

protein	ν_{Fe-His} cm^{-1}	ν_{Fe-CO} cm^{-1}	ν_{Fe-OO} cm^{-1}	ref
Mt-trHbO	226	525	559	(*23*)
Mt-trHbO Y(B10)F	226	525	559	(*23*)
Mt-trHbO Y(CD1)F	226	515	556	(*23*)
Mt-trHbO W(G8)F	226	514 497	563	*a*
Mt-trHbO Y(CD1)F/W(G8)F	226	497	563	*a*
Mt-trHbN	226	535 500	560	(*34*)
Mt-trHbN Y(B10)F	226	502	570	(*34*)
Chlamydomonas LI637	232	491	554	(*43*)
Synechocystis PCC6803	nd[b]	492	554	(*44*)
Paramecium caudatum	220	493	563	(*45*)
Cj-trHbP	226		542	(*35*)
Cj-trHbP Y(B10)F			552	(*35*)
Cj-trHbP H(E7)L			550	(*35*)
Cj-trHbP Y(B10)F/H(E7)L			557	(*35*)

[a] This work. [b] Not determined.

hydrogen bond (3.3 Å) weakly connects Y(CD1) to W(G8); in *Bs*-trHbO Y(B10) is hydrogen bonded to the carbonyl group of Q(E11) (hydrogen bond of 3.0 Å), the cyanide ligand−W(G8) distance being 3.4 Å (*1*, *10*).

Kinetic studies on group II trHbs have revealed distinct ligand binding properties resulting in very different O_2 affinities (Table 2) (*2*, *10*, *12*, *13*), which may reflect adaptations to function in the different environment in which the different organisms are found. At present the role of the individual distal residues in the ligand binding reaction has been reported, in part, only for *Mt*-trHbO (*2*). Substitution of Y(B10) for Phe showed no significant kinetic effect on either binding or dissociation of O_2 and CO. Changing Y(CD1) for Phe caused a 25-fold increase in the O_2 combination rate, but almost no change in the O_2 dissociation rate. On the contrary, the functional role of W(G8) has not been investigated, notwithstanding the fact that W(G8) is an invariant residue in group II and group III trHbs (Val/Leu in group I) (*7*, *9*), that has no counterpart in vertebrate Hbs (*14*). The crystal structures show that in *Mt*-trHbO, in *Bs*-trHbO, in *Tf*-trHbO, in *Gs*-trHbO, and in group III *Cj*-trHbP residue W(G8) is parallel and in contact with the heme, filling the inner part of the distal heme pocket. Additionally, W(G8) occupies most of the protein matrix short tunnel branch observed in (group I) *Mt*-trHbN, converting the long tunnel branch (that links the heme cavity to the solvent and may be used for ligand diffusion) into two small cavities (*15*, *16*).

In the present work we characterize the structural properties of the W(G8)F and Y(CD1)F/W(G8)F *Mt*-trHbO mutants through optical absorption and resonance Raman spectroscopy, obtained under different oxidation states and ligand binding conditions. The functional properties, determined by measuring the ligand binding constants, are interpreted at the light of the crystal structure of the W(G8)F *Mt*-trHbO mutant, here reported at 1.9 Å resolution.

MATERIALS AND METHODS

Mutagenesis, Expression, and Purification. Amino acid substitutions were carried out using the QuikChange Site-Directed Mutagenesis kit (Stratagene) following the recommended protocol. The cloned *M. tuberculosis glbO* gene was used as a template with the complementary oligonucleotide primers Y(CD1)F, 5′CTGCG GCGGGTGTTCCCCGAAGATGAC3′ with 5′GTCATCTTCGGGGAACACCCGCCGCAG3′; W(G8)F, 5′GAACGCGACGCCTTTCTGCGGTGCATG3′ with 5′CATGCACCGCAGAAAGGCGTCGCGTTC3′. Wild-type recombinant *Mt*-trHbO and its Y(CD1)F, W(G8)F, and Y(CD1)/W(G8)F mutants were prepared as described previously (*2*).

Electronic Absorption Spectra of the Ferric Proteins. Optical absorption spectra were recorded using a Cary 3E spectrophotometer (Varian, Mississauga, Canada) equipped with a temperature-controlled multicell holder. Samples of ferric proteins at a concentration of 10 μM were prepared in the following buffers: sodium acetate (pH 5.0), potassium phosphate (pH 7.5) and CAPS-NaOH (pH 10.5). All buffer concentrations were 50 mM, and the solutions contained 50 μM EDTA. The spectra were recorded at 23 °C and analyzed using the Kaleidagraph software (Synergy Software).

Denaturation in the Presence of Guanidium Chloride. A stock 7.0 M guanidium chloride (GdmCl) solution was prepared in 200 mM potassium phosphate buffer (pH 7.0) containing 50 μM EDTA. The appropriate volume of buffer and stock GdmCl were mixed to give the desired GdmCl concentration (0−5 M) in a final volume of 1 mL. The electronic absorption spectra were recorded (250−700 nm) from two matched 1.5 mL quartz cuvettes at 23 °C. A baseline spectrum was recorded at all GdmCl concentrations tested. To initiate the reactions concentrated ferric HbO was added to the sample cuvette at a final concentration of 10 μM and unfolding reactions were allowed to reach equilibrium. Soret absorbance values were plotted as a function of GdmCl concentration. The titration data were fitted to a simple two-state unfolding reaction, protein ↔ denatured with a single equilibrium constant, $K_{Prot,D}$ (*17*), where $K_{Prot,D}$ is the isomerization constant for denaturation of the holoprotein in buffer.

Resonance Raman Spectroscopy. Resonance Raman spectroscopy was performed as described previously (*18*). Briefly, protein samples at a concentration of 50 μM were buffered in 50 mM potassium phosphate (pH 7.5) containing 50 μM EDTA. The deoxy protein samples were prepared by injecting a 10-fold molar excess of sodium dithionite to argon-equilibrated protein samples in tightly sealed Raman cells. CO derivatives were prepared by exposing argon-equilibrated, dithionite-reduced protein samples to $^{12}C^{16}O$ (MEGS inc, Quebec, Canada), $^{12}C^{18}O$, or $^{13}C^{18}O$ (Icon Isotopes, Summit, NJ). To obtain the O_2 derivatives, the deoxy protein samples were prepared inside an anaerobic glovebox as described further below. The O_2 derivatives were prepared by injecting either $^{16}O_2$ (Praxair, Quebec, Canada) or $^{18}O_2$ (Cambridge Isotopes Laboratories, Andover, MA) to the dithionite-free deoxy protein samples. The output at 441.6 nm from a He/Cd laser was used to acquire the spectra of the deoxy derivatives. The excitation source for the acquisition of the O_2 and CO spectra was the 413.1 nm line of a krypton ion laser maintained at a power of less than 2 mW to minimize ligand dissociation. All measurements were made at room temperature. Cosmic ray lines were removed from the spectra by a routine of Winspec software (Roper Scientific, Princeton, NJ). Several 5 min spectra were acquired over a 30 min period and analyzed using the Grams/AI software (ThermoGalactic).

Table 2: Kinetics Constants for the Reactions of *Mt*-trHbO and Its Mutants with O_2 and CO

	k'_{on} (O_2) μM^{-1} s^{-1}	k'_{off} (O_2) s^{-1}	l'_{on} (CO) μM^{-1} s^{-1}	l'_{off} (CO) s^{-1}	ref
Mt-trHbO	0.11 (80%) 0.85 (20%)	0.0014 (78%) 0.0058 (22%)	0.0137 (79%) 0.180 (21%)	0.0040 (60%) 0.0015 (40%)	(*2*)
Mt-trHbO Y(B10)F	0.067 (95%) (5%)[a]	0.0026 (50%) 0.0058 (50%)	0.013 (95%) (5%)[a]	0.023 (56%) 0.0059 (44%)	(*2*)
Mt-trHbO Y(CD1)F	2.7 (95%) 11.5 (5%)	0.0093 (75%) 0.0052 (25%)	1.06 (95%) (5%)[a]	0.0064 (70%) 0.0015 (30%)	(*2*)
Mt-trHbO W(G8)F	12.7 ± 0.783	1.03 ± 0.01 (55%) 0.066 ± 0.003 (45%)	3.71 ± 0.0784 (75%) 1.17 ± 0.0797 (25%)	0.027 (31%) 0.0095 (40%) 0.0004 (29%)	this work
Mt-trHbO Y(CD1)F/W(G8)F	22.9 ± 1.07	0.0915 ± 0.0013	11.2 ± 1.19	0.00425 ± 0.0005 (74%) 0.0010 ± 0.0006 (26%)	this work
Mt-trHbN	25.0	0.199	6.75	0.005	(*46*)
Mt-trHbN Y(B10)F		30			(*46*)
At-trGLB3	0.2	0.3	0.014	0.001	(*13*)
Bs-trHbO	14.0	0.002	0.22	0.00046	(*10*)
Gs-trHbO	76.5	0.0058	0.38	0.00056	(*11*)
Tf-trHbO	0.9	0.07			(*12*)
Cj-trHbP	0.91	0.0041			(*35*)
Cj-trHbP Y(B10)F	0.12	0.0088			(*35*)
Cj-trHbP H(E7)L	0.49	0.0003			(*35*)
Cj-trHbP Y(B10)F/H(E7)L	42	0.0028			(*35*)

[a] Rates are independent of ligand concentration and heterogeneous.

Determination of Ligand Reaction Rates. Rapid mixing experiments were conducted with an Applied Photophysics SX18MV single-wavelength stopped-flow spectrophotometer (Leatherhead, U.K.). To reproducibly achieve satisfactory anaerobic conditions, sample preparation and stopped-flow spectrophotometric experiments were carried out in a glovebox (LabMaster100, MBraun Inc.), equipped with a catalytic purifier that maintained the oxygen content at ~3 ppm, as described previously (*2*).

Crystal Structures. The purified *Mt*-trHbO mutant proteins (W(G8)F, Y(CD1)F, Y(CD1)F/W(G8)F) were crystallized adapting the methods previously described for the wild-type protein (*1*). Briefly, each protein solution at a concentration of 15 mg/mL was assembled in sitting drop vapor diffusion crystallization experiments against reservoir solutions containing 2.2 M ammonium sulfate, 0.05 M phosphate buffer, 0.001 M KCN, pH 7.2. Each crystallization droplet was composed of 0.5 μL of the protein stock solution and 0.5 μL of the reservoir solution. The drops were equilibrated against the reservoir buffer at 4 °C for 2−3 weeks for the W(G8)F mutant, and for approximately 8 weeks for the other two mutants. X-ray diffraction data were collected at the ESRF (Grenoble, France), beam line ID14-3, at 100 K, using flash-cooled crystals that had been rapidly transferred to a medium containing 20% glycerol, 2.85 M ammonium sulfate, 0.001 M KCN, 0.05 M phosphate buffer, pH 7.2. All the mutant crystals isolated are isomorphous with those of the wild-type *Mt*-trHbO (tetragonal space group $I4_122$; see Table 3), thus containing 12 *Mt*-trHbO chains per asymmetric unit. However, crystals of both the Y(CD1)F and Y(CD1)F/W(G8)F mutants displayed only low resolution diffraction (<4 Å), and rapidly decayed under X-ray exposure. Data reduction and scaling for the W(G8)F mutant was carried over using Mosflm/SCALA and programs from the CCP4 suite (*19, 20*). Since low resolution diffraction was systematically observed for several different crystals of the Y(CD1)F and Y(CD1)F/W(G8)F *Mt*-trHbO mutants, grown in three different batches over 6 months, crystallographic analysis of these two mutants was no longer pursued.

Table 3: X-ray Data Collection and Refinement Statistics for the Mt-trHbO W(G8)F Mutant

Data Collection Statistics	
space group	$I4_122$
unit-cell parameters (Å)	$a = b = 187.3$ Å, $c = 274.5$ Å
resolution range (Å)	48−1.93
mosaicity (deg)	0.2
no. of unique reflections	178559 (23850)[a]
completeness (%)	98.7 (91.4)[a]
redundancy	4.8 (3.5)
R_{merge}[b] (%)	7.8 (45.5)
average $I/\sigma(I)$	13.7 (2.3)
Refinement Statistics	
R factor[c] (%)	16.7
R_{free}[d] (%)	20.9
rms bond lengths (Å)	0.10
rms bond angles (deg)	1.15
Ramachandran Plot	
resid in most fav reg (%)	94.0
resid in add. allow. reg (%)	6.0

[a] High-resolution shell: 2.01−1.91 Å. [b] $R_{merge} = \sum|I - (I)|/\sum I \times 100$, where I is intensity of a reflection and (I) is the average intensity. [c] R factor $= \sum|F_o - F_c|/\sum|F_o| \times 100$. [d] R_{free} is calculated from 5% randomly selected data for cross-validation.

Table 4: Heme−Fe Coordination Geometry in the W(G8)F *Mt*-trHBO Mutant Structure (Average Values)

Fe−CN (Å)	2.0 ± 0.1[a]
Fe−C−N (deg)	162 ± 11[a]
Y(CD1)(OH)−CN (Å)	2.71 ± 0.09[a]
HF8(Nε2)−Fe (Å)	2.10 ± 0.03

[a] Excluding subunit E (Fe−CN = 2.49 Å).

After rigid body refinement of the 12 asymmetric unit protein chains of the W(G8)F mutant, the crystal structure was refined using REFMAC, and the models inspected/modified using O (*21*). The final refinement parameters are listed in Tables 3 and 4. Atomic coordinates and structure factors for the W(G8)F *Mt*-trHbO mutant have been deposited with the Protein Data Bank (*22*) with accession code 2QRW.

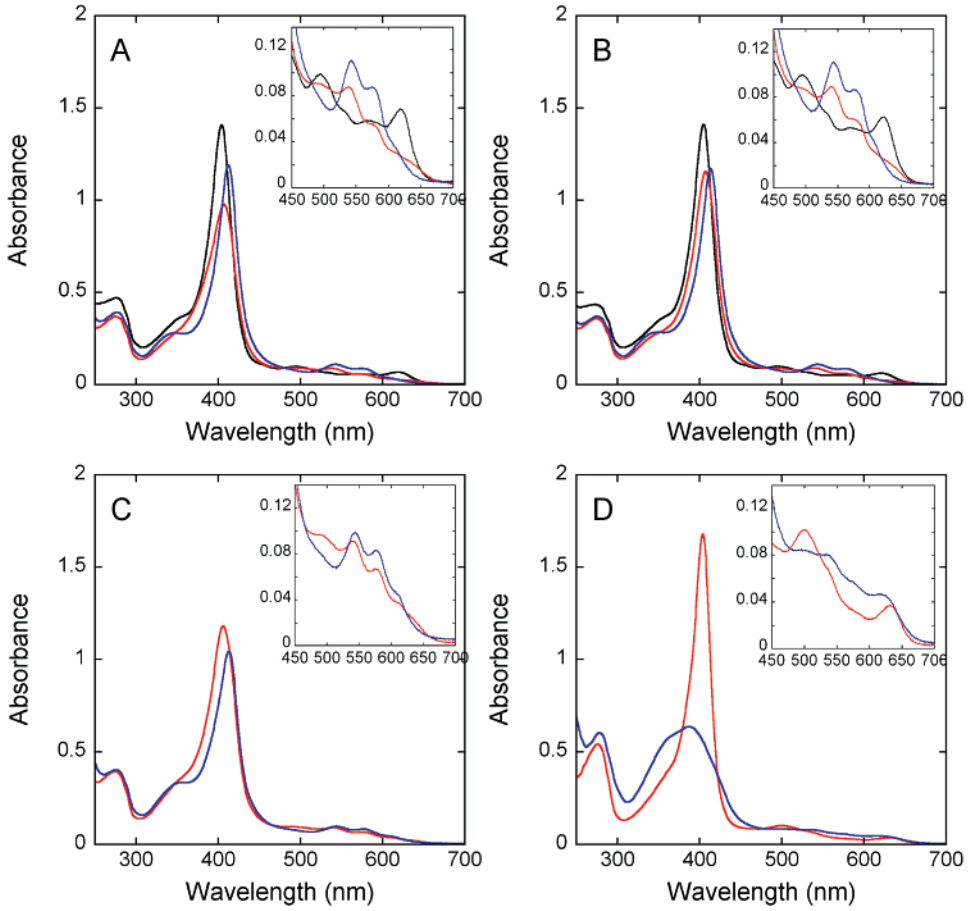

FIGURE 1: The pH dependence of the absorption spectra of (A) the met forms of *Mt*-trHbO and their variants (B) Y(CD1)F, (C) W(G8)F, and (D) Y(CD1)F/W(G8)F. Spectra at pH 5 (black), 7.5 (red), and 10.5 (blue) were recorded at 23 °C.

RESULTS

Electronic Absorption Spectra of the Ferric Proteins. Figure 1 compares the electronic absorption spectra of the ferric derivatives of *Mt*-trHbO, the single mutants Y(CD1)F and W(G8)F, and the double mutant Y(CD1)F/W(G8)F at pH 5.0, 7.5, and 10.5. As previously reported, the ferric form of wild-type *Mt*-trHbO at neutral pH represents a mixture of low- and high-spin heme with maxima at 407, 493, 539, 577 and a shoulder at 620 nm (*23*). Changing the Y(CD1) residue for a phenylalanine resulted in a spectrum almost identical to the wild-type protein except that the Soret band showed higher absorbance. The optical spectrum of the W(G8)F mutant also indicated a mixture of low-spin and high-spin species except that the Soret band was slightly blue-shifted to 405 nm and showed higher absorbance than that of wild-type protein. At neutral pH, the optical spectrum of the ferric complex of the double mutant Y(CD1)F/W(G8)F was primarily six coordinate high-spin heme as indicated by the electronic transition at 403 nm and the charge-transfer band (CT1) at 633 nm.

At pH 10.5, all proteins, except the Y(CD1)F/W(G8)F mutant, exhibited a typical spectrum of a six coordinate low-spin hydroxy met form with maxima at 412, 540, and 577 nm. In contrast, the Soret band of the double mutant was shifted to 389 nm and showed a significant decrease in absorbance indicating a transition from a six coordinate high-spin species to a five coordinate high-spin species.

At pH 5.0, the optical absorption spectra of the ferric complexes of *Mt*-trHbO and Y(CD1)F mutant were typical of a six coordinate aqua-met spectrum as revealed by the positioning of the Soret band at 405 nm and maxima at 500 and 630 nm in the visible region. The W(G8)F and Y(CD1)F/W(G8)F mutants underwent denaturation and precipitation at acidic pH.

Guanidium Experiments. The impact of the substitutions at the CD1 and G8 positions on protein stability was further investigated by measuring resistance of the holoproteins to denaturation in the presence of GdmCl. A comparison of the melting curves in the presence of GdmCl for the met forms of *Mt*-trHbO and the variants Y(CD1)F and W(G8)F is shown in Figure 2. The GdmCl concentration required to denaturate half of the proteins was 3.0, 2.6, and 1.6 M GdmCl for *Mt*-trHbO, Y(CD1)F, and W(G8)F, respectively. The data were fitted to a simple two-state unfolding reaction, protein $\leftrightarrow$ denatured with a single equilibrium constant, $K_{Prot,D}$ (*17*). The calculated relative stabilities ($1/K_{Prot,D}$) of the different proteins are *Mt*-trHbO (1.4×10^{-6}) $\approx$ Y(CD1)F (6.2×10^{-6}) $>>>$ W(G8)F (382×10^{-6}). These results argue for a structural role for W(G8) in *Mt*-trHbO.

Resonance Raman Spectra of the Deoxy Derivatives. The high-frequency region (1300−1700 cm^{-1}) of the resonance Raman spectra of heme proteins are composed of several porphyrin in-plane vibrational modes, which are sensitive to the oxidation, coordination, and spin-state of the heme iron (*24*, *25*). Figure 3A shows the spectra of the deoxy derivatives of *Mt*-trHbO and the variants W(G8)F and Y(CD1)F/W(G8)F in the high-frequency region at pH 7.5. The marker bands $\nu 4$ at 1356 cm^{-1} and $\nu 3$ at 1471 cm^{-1} are

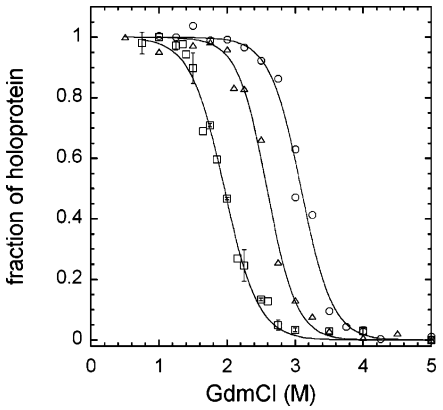

FIGURE 2: Fraction of holoprotein deduced from changes in the Soret absorbance resulting from the unfolding of met *Mt*-trHbO and its variants Y(CD1)F, and W(G8)F as function of GdmCl concentration. Spectra at pH 7 were recorded at 23 °C. The buffer used was potassium phosphate, pH 7. Symbols: *Mt*-trHbO (circle), Y(CD1)F (triangle), and W(G8)F (square).

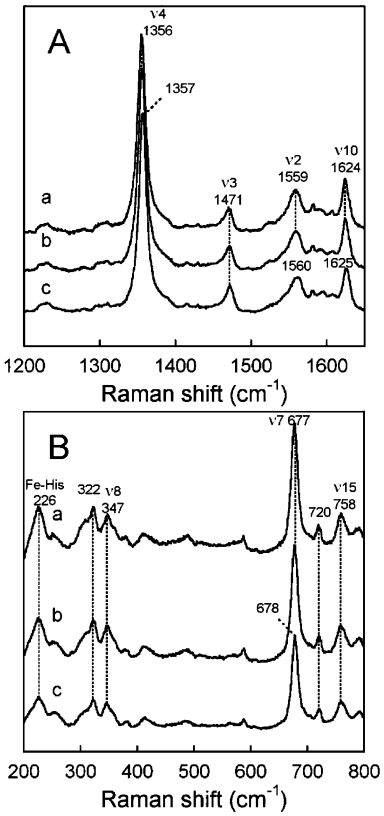

FIGURE 3: Resonance Raman spectra of the deoxy forms of *Mt*-trHbO and its variants W(G8)F and Y(CD1)F/W(G8)F at pH 7.5 in the high (A) and low (B) frequency region: a, Y(CD1)F/W(G8)F; b, W(G8)F; c, *Mt*-trHbO. The excitation wavelength was 442 nm.

characteristic of a five coordinate high-spin deoxy heme, which is consistent with their optical spectra (not shown).

The low-frequency region of the resonance Raman spectra of heme proteins contains the vibrational modes associated with the coordinated ligands of the heme iron (*24*, *25*). The assignment of a ligand vibrational mode is extremely useful as it directly identifies a particular ligand and the nature of its interactions with amino acid residues in the heme pocket. In particular, the proximal Fe−His stretching mode (ν_{Fe-His}) can be identified in the 5C deoxy forms of hemoglobins in the 200−250 cm^{-1} region. The frequency of the ν_{Fe-His} mode

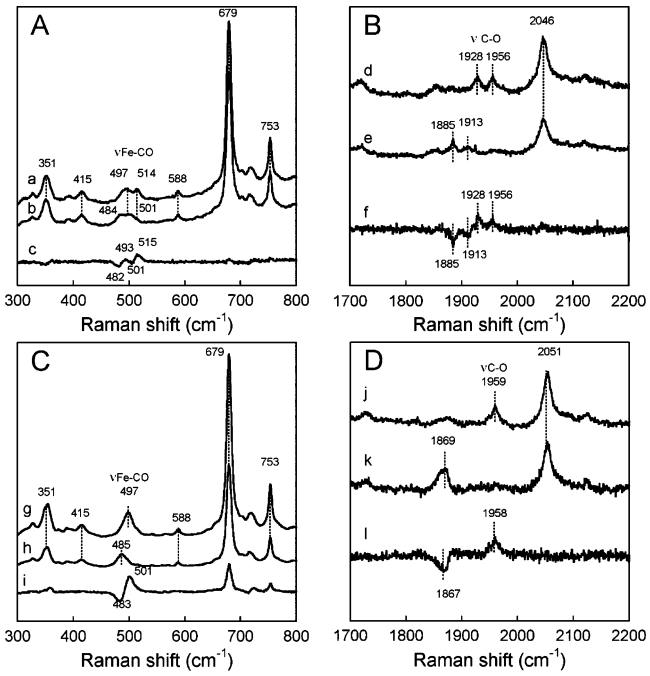

FIGURE 4: Resonance Raman spectra of the CO derivatives in the low- and high-frequency regions of the W(G8)F (panels A and B) and Y(CD1)F/W(G8)F (panels C and D) mutants at pH 7.5: a, W(G8)F-^{12}C^{16}O; b, W(G8)F-^{12}C^{18}O; d, W(G8)F-^{12}C^{16}O; e, W(G8)F-^{12}C^{18}O; g, Y(CD1)F/W(G8)F-^{12}C^{16}O; h, Y(CD1)F/W(G8)F-^{13}C^{18}O; j, Y(CD1)F/W(G8)F-^{12}C^{16}O; k, Y(CD1)F/W(G8)F-^{13}C^{18}O; traces c and f correspond to the difference spectrum ^{12}C^{16}O minus ^{12}C^{18}O; traces i and l correspond to the difference spectraum ^{12}C^{16}O minus ^{13}C^{18}O for each protein.

of the deoxy form at pH 7.5 of both mutants was found nearly identical to that of *Mt*-trHbO at 226 cm^{-1} (Figure 3B, Table 1).

Resonance Raman of CO-Bound Ferrous Complexes. The Fe−CO stretching mode (ν_{Fe-CO}) is sensitive to the nature of distal interactions with CO and is also dependent on the nature of the proximal ligand to the heme (*26*).

Figures 4A and 4C show the low-frequency region of the resonance Raman spectra of the CO adduct of the W(G8)F and Y(CD1)F/W(G8)F mutants. Each of these assignments was confirmed by isotope (^{12}C^{18}O or ^{13}C^{18}O) substitution experiments. The single mutant W(G8)F displayed two ν_{Fe-CO} modes at 497 cm^{-1} and 514 cm^{-1}, which shifted to 484 and 501 cm^{-1}, respectively, with ^{12}C^{18}O. This singly labeled isotope was used since with ^{13}C^{18}O, a ν_{Fe-CO} at 498 cm^{-1} overlapped with the mode at 497 cm^{-1} of ^{12}C^{16}O thus rendering the isotope shift less clear (not shown). The two ν_{Fe-CO} modes at 497 and 514 cm^{-1} can be assigned to two conformers. For the conformer with the stretching mode at 514 cm^{-1}, CO possibly interacts with the Y(CD1) since this band is no longer detected in the double mutant (Figure 4C). The stretching frequency of this conformer is lower than that of *Mt*-trHbO (525 cm^{-1}) (Table 1) and suggests that the W(G8) is in close contact with the bound CO. The second ν_{Fe-CO} mode at 497 cm^{-1} of the W(G8)F mutant, which is identical to that of the Y(CD1)F/W(G8)F mutant, suggests a heme pocket architecture in which there is no or little polar interaction between distal residues and the heme-bound CO (*26*, *27*).

In the high-frequency region (Figure 4B, 4D), two C−O stretching modes (ν_{C-O}) at 1928 and 1956 cm^{-1} were

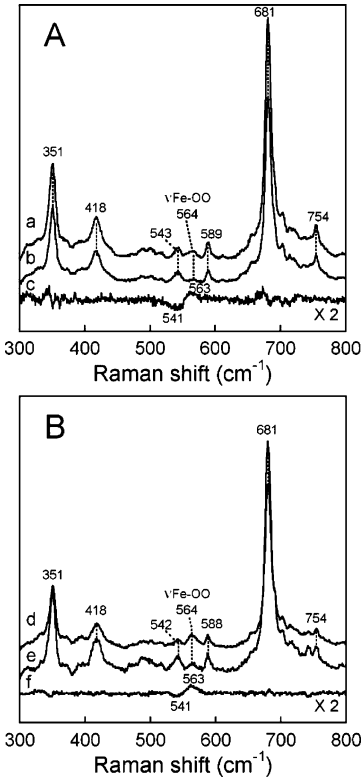

FIGURE 5: Low-frequency region of the resonance Raman spectra of the O_2 derivatives of the W(G8)F (panel A) and Y(CD1)F/W(G8)F (panel B) mutants: a, W(G8)F-$^{16}O_2$; b, W(G8)F-$^{18}O_2$; d, Y(CD1)F/W(G8)F-$^{16}O_2$; e, Y(CD1)F/W(G8)F-$^{18}O_2$; c and f correspond to the difference spectra ^{16}O minus ^{18}O for each protein.

detected for the W(G8)F mutant. The 43 cm^{-1} isotopic shifts between the bands located at 1956 cm^{-1} ($^{12}C^{16}O$) and 1913 cm^{-1} ($^{12}C^{18}O$) and those located at 1928 cm^{-1} ($^{12}C^{16}O$) and 1885 cm^{-1} ($^{12}C^{18}O$) in the W(G8)F mutant difference spectrum (Figure 4B) are close to the expected shift based on a diatomic C−O oscillator and were thus assigned to ν_{C-O} modes. The ν_{C-O} modes at 1928 and 1956 cm^{-1} are associated with the ν_{Fe-CO} modes at 514 and 497 cm^{-1}, respectively, and fall on the ν_{Fe-CO} versus ν_{C-O} correlation line of histidine-coordinated heme proteins (not shown). A single C−O stretching mode was detected at 1959 cm^{-1} for the Y(CD1)F/W(G8)F mutant (Figure 4D). The magnitude of the ν_{C-O} isotopic shift was 91 cm^{-1} upon substitution with $^{13}C^{18}O$, very close to the 90 cm^{-1} isotopic shift expected for a diatomic oscillator. Taken together resonance Raman data indicate that in *Mt*-trHbO both Y(CD1) and W(G8) residues are interacting with the heme bound CO presumably through hydrogen-bonding with the oxygen atom of the bound CO.

Resonance Raman of O_2-Bound Ferrous Complexes. The oxy complexes of the *Mt*-trHbO mutants were studied by resonance Raman spectroscopy in order to assign the Fe−O_2 stretching mode (ν_{Fe-OO}) and to determine its sensitivity to the environment in the distal heme pocket.

Figures 5A and 5B compare the low-frequency region of the resonance Raman spectra of the oxygenated W(G8)F and Y(CD1)F/W(G8)F mutants, respectively. The Fe−O_2 band was broad and centered at 564 cm^{-1} for the two mutants. Upon $^{18}O_2$ isotopic substitution, the line at 564 cm^{-1} disappeared and the intensity of a line at 542 cm^{-1}, that overlaps a heme mode at 542 cm^{-1}, was observed (Figures 5A and 5B). The difference spectra clearly showed these shifts and allowed the assignment of the line at 564 cm^{-1} of both mutant proteins to the Fe−O_2. The magnitude of the isotopic shift (21 and 22 cm^{-1} for the W(G8)F and the Y(CD1)F/W(G8)F mutant, respectively) is very close to that expected for a Fe−O diatomic oscillator (24 cm^{-1}). The higher stretching frequency of the Fe−O_2 mode observed in both mutants (564 cm^{-1}) in comparison with *Mt*-trHbO (559 cm^{-1}) is consistent with the loss of hydrogen bonding between the indole Nϵ1 atom of W(G8) and the *proximal* oxygen atom of the heme-bound O_2. However, the Fe−O_2 frequency is still low compared to that recorded in vertebrate myoglobins and hemoglobins (~570 cm^{-1}) where there is no constraint on the proximal oxygen atom. Since the crystal structure of the CN-bound form of the W(G8)F mutant revealed that there is no strong hydrogen bond interaction of the CN ligand with the Y(B10), it appears more likely that the low frequency of the ν_{Fe-OO} mode observed in both W(G8) mutants is caused by the positive edge of the F(G8) phenyl multipole that interacts with the iron-bound O_2. Such productive electrostatic interaction has also been described in the myoglobin L(B10)F mutant (*28*−*30*) and in the *Mt*-trHbN Y(B10)F mutant (*18*).

O_2 Binding. The combination rates for O_2 binding of the two mutant proteins were measured by rapid mixing but on a relatively small range of O_2 concentrations due to fast reactions. The combination rates could not be measured by laser photolysis, as no ligand photodissociation was detected using a 5 ns flash (results not shown). For the single mutant W(G8)F the time courses were better fitted with two exponentials. The slow component showed apparent pseudo-first-order kinetics, and the bimolecular rate constant (k'_{on}) was 12.7 μM^{-1} s^{-1} (Figure 6A) (Table 2). The rate of the fast population was too rapid to be measured accurately by stopped-flow spectrometry. The reaction between the deoxy Y(CD1)F/W(G8)F protein and O_2 was monophasic. The observed pseudo-first-order rate constant was directly proportional to the O_2 concentration, and the k'_{on} was 22.9 μM^{-1} s^{-1}. This second-order rate constant is more than 100-fold greater than that of *Mt*-trHbO (Table 2).

O_2 Dissociation. Replacement of O_2 by CO in the single mutant W(G8)F showed two rates of almost equal amplitude (1.03 s^{-1} and 0.066 s^{-1}). Both are very much faster than those of wild-type, suggesting that the W(G8) participates in the stabilization of the heme-bound O_2 (Table 2). Interestingly, replacement of O_2 in the double mutant was monophasic and the rate was increased to 0.091 s^{-1}, 64-fold greater than that of the major component in the wild-type protein. It is noteworthy that changing both Y(CD1) and W(G8) for Phe has only an intermediate effect on the O_2 dissociation rate in comparison with the W(G8)F mutant. Consistent with the resonance Raman data this result suggests that the bound O_2 is still stabilized even in the absence of H-bonding with Y(CD1) and W(G8), which may be attributed to the interactions with the positive edge of the phenyl multipole.

CO Binding. The CO combination rates of the single mutant W(G8)F and the double mutant Y(CD1)F/W(G8)F were measured using stopped-flow spectrophotometry (Table 2). CO combination with the deoxy W(G8)F mutant showed two components whose rates increased linearly with ligand concentrations, whereas CO combination with the double mutant was monophasic. Second-order combination rate

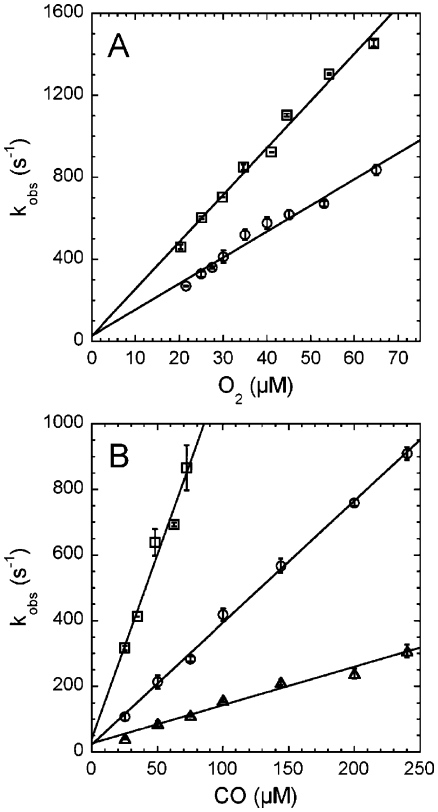

FIGURE 6: O_2 and CO binding to ferrous deoxy W(G8)F and Y(CD1)F/W(G8)F mutants. Dependence of the observed association rates on O_2 (A) and CO (B) concentration determined by rapid mixing at pH 7.5, 23 °C. Symbols: Y(CD1)F/W(G8)F mutant (square), W(G8)F major rate (circle), and W(G8)F major rate (triangle).

constants (l'_{on}) for each mutant were obtained from slopes of the linear fits of the observed k_{obs} versus CO concentration (Figure 6B). For the W(G8)F mutant, the major (75%) and the minor (25%) components exhibited apparent second-order rate constants of 3.71 and 1.17 μM^{-1} s^{-1}, respectively. The apparent second-order rate constant value of the double mutant further increased to 11.2 μM^{-1} s^{-1}, which is 817-fold greater than that of the major component of the wild-type protein (Table 2).

CO Dissociation. The CO dissociation rate was measured by replacement with O_2. As summarized in Table 2, the time courses of the kinetics of the single mutant W(G8)F were better fitted with three exponentials of almost equal amplitude. The observed rates are as low as those of the wild-type protein, except for one third of the population, which showed a 10-fold increase in l'_{off}. The observed rates and amplitudes of the Y(CD1)F/W(G8)F were similar to those of *Mt*-trHbO.

Structure of the W(G8)F Mutant. The cyano-met W(G8)F mutant crystal structure was refined to final R_{gen}/R_{free} values of 16.7% and 20.9%, respectively, at 1.93 Å resolution (Table 3). As for the wild-type protein, the twelve asymmetric unit chains are assembled in a compact dodecamer displaying approximate 32 point group symmetry (*1*). Additionally, as previously observed, six of the twelve chains (the "vertex" subunits (*1*)) display a covalent bond linking residues Y(B10) and Y(CD1) through an ether bond that is based on the phenolic O atom of residue Y(B10). Such covalent modification is absent in the remaining six "side" subunits of the dodecameric assembly. The mutant protein backbone is virtually unaffected by the W(G8)F mutation; the rmsd calculated between the Cα atoms of the wild-type and mutated proteins fall in the 0.2 Å range when the six dodecamer "vertex" subunits are overlaid. Similar results are found when the wild-type and mutant dodecamer "side" subunits are considered. Conversely, the rmsd is higher (about 0.8 Å) when vertex subunits are compared with side subunits; such a pattern of structural differences had been noted earlier within the *Mt*-trHbO dodecamer. As a result, the quaternary assembly of *Mt*-trHbO itself is essentially unaffected by the mutation.

At the G8 site the W→F mutation does not significantly affect the backbone conformation; the mutated Phe side chains matches closely the conformation adopted by W(G8) in the wild-type protein, being parallel to the porphyrin ring at a stacking distance of 3.5 Å. The G8 phenyl ring sits approximately in the center of mass of the indole of the substituted Trp residue (Figure 7A). Likely due to the decreased size of the G8 side chain, residue M(G12) readjusts slightly, to fill the cavity created by W(G8) substitution (shifts of 0.4−0.6 Å, according to the subunit considered). A similar shift (0.4−0.5 Å) is observed in residue L(H11), falling at 3.8 Å from the indole ring of W(G8) of the wild-type protein. In the "side" *Mt*-trHbO subunits, devoid of the Y(B10)−Y(CD1) covalent link, the latter two Tyr residues also move slightly (0.6−0.7 Å), likely reflecting the removal of a van der Waals contact between phenolic O atom and the W(G8) indole ring. Such readjustment is absent, or comparable to the rmsd, in the "vertex" subunits where Y(B10) and Y(CD1) are covalently linked. Conformational differences between the wild-type protein and the W(G8)F mutant are observed in the CD region, centered around residue E(CD3), whose Cα atom deviates by 2.5−3.5 Å from the wild-type protein structure in the different "vertex" subunits; such deviation is virtually absent in the "side" subunits. Such structure discrepancy between the two types of subunits in the mutated protein may be promoted by the W(G8)F mutation that allows Y(CD1) and Y(B10) to readjust differently within the heme distal pocket in relation to the absence/presence of a covalent link between the two residues.

Despite the loss of one hydrogen bond to W(G8) indole, the coordination geometry of the cyanide ligand is little affected by the mutation (within the resolution limits of the available data; see Table 4). Thus, besides the coordination bond to the heme Fe atom, the ligand is hydrogen bonded, through the cyanide distal N atom, to the Y(CD1) phenolic O (average distance 2.7 Å), irrespective of the presence or absence of the Y(B10)−Y(CD1) covalent link. The main structural difference between "vertex" and "side" subunits, in the W(G8)F mutant protein, concerns the additional ligand stabilization provided by Y(B10), that offers a weak hydrogen bond (average 3.4 Å) to the distal N atom of cyanide only in the "vertex" subunits. In the absence of the Tyr-Tyr post-translational modification (side subunits), such stabilizing interaction is lost, with a cyanide−Y(B10) phenolic O average distance of 4.4 Å.

DISCUSSION

The presence of Y(B10), Y(CD1), and W(G8) residues makes the distal site of *Mt*-trHbO unique within the globin

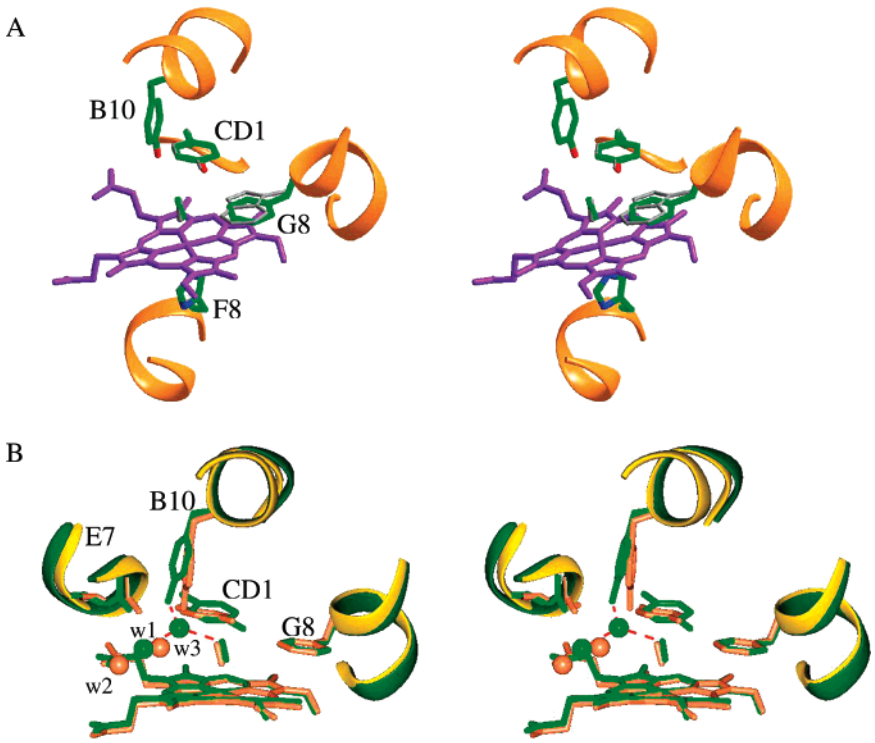

FIGURE 7: Stereoview of *Mt*-trHbO distal site. A: The figure shows the heme region (the distal site area is in the foreground) together with short helical stretches, and key functional residues, shown in green for the W(G8)F mutant; residue W(G8) of the wild-type protein is shown in gray. The cyanide ligand is also displayed as a short segment coordinated to the heme Fe atom. B: Structural overlay of the distal site region for W(G8)F mutant, "vertex" molecule (orange bonds/yellow ribons), and "side" molecule (green bonds/dark green ribons), also displaying the water molecules (W1−W3) filling the proposed site of access to the heme distal region from the solvent. The figures were generated using CCP4mg (*47*).

family. Here we investigated the role of W(G8) in ligand binding to *Mt*-trHbO. Since crystallographic investigations showed that Y(CD1) interacts with the bound ligand and with W(G8), a mutant harboring substitutions at both positions was also examined.

Equilibrium constants for GdmCl-induced denaturation of *Mt*-trHbO, Y(CD1)F, and W(G8)F holoproteins indicated that the W(G8)F mutant is less stable than the wild-type protein suggesting a structural role for the latter residue. In contrast, the $K_{Prot,D}$ value for the Y(CD1)F mutant is very similar to that of *Mt*-trHbO. Heme stabilizes Mb and Hb with respect to their corresponding apoglobins (*17*, *31*, *32*). The W(G8) residue may thus stabilize *Mt*-trHbO through efficient van der Waals contacts to the porphyrin ring, but also by filling an apolar core cavity that would be left empty by any G8 residue smaller than Trp. In addition, the W(G8)F mutant was found to be unstable at acidic pHs, which also supports a structural role for this residue. In contrast, the Y(CD1)F mutant is as stable as *Mt*-trHbO under acidic conditions. The optical spectrum of the met form of the Y(CD1)F/W(G8)F mutant at alkaline pH is typical of ferric proteins in which the sixth coordination position is vacant suggesting that both residues stabilize the bound hydroxide in *Mt*-trHbO.

Resonance Raman of the Ferrous Unliganded Form. Resonance Raman analyses indicated that the distal heme environment of the ferrous unliganded form of the W(G8) mutants is comparable to that of *Mt*-trHbO (Figure 3 and Table 1) (*23*). In addition the Fe−His stretching mode of the mutants is not affected, suggesting that the chemical nature of the proximal Fe−His bond is not perturbed. As observed in *Mt*-trHbO the high frequency of the Fe−His stretching mode indicates no or weak proximal strain on the Fe−His bond in the mutant proteins.

Interactions of Y(CD1) and W(G8) with the Bound CO. Previous resonance Raman studies of the CO form of *Mt*-trHbO revealed a single Fe−CO stretching mode 525 cm^{-1}, a value that is higher than in most globins (Table 1) that indicates that the bound-heme CO interacts strongly with the distal polar residues (*23*). When Y(CD1) was substituted by Phe, the Fe−CO stretching mode was shifted-down to 515 cm^{-1}, which is still 15−25 cm^{-1} higher than that of a heme-bound CO experiencing no polar interactions (*26*). Substitution of Y(B10) by Phe did not change the Fe−CO stretching frequency but caused broadening of the peak indicating that the distal environment of the heme-bound CO was comparable to that of *Mt*-trHbO; however, the conformational freedom of the heme-bound CO was considerably increased (*23*). We had postulated that, in the absence of Y(CD1), Y(B10) can interact with the heme-bound CO through a relatively less favorable hydrogen-bonding interaction as indicated by the downshift of the Fe−CO stretching frequency. Here we showed that changing W(G8) for Phe causes the appearance of two Fe−CO stretching modes at 514 cm^{-1} and 497 cm^{-1}. The lower Fe−CO stretching frequency at 497 cm^{-1} is attributed to a conformation with no or very weak hydrogen-bonding interactions and characteristic of a less positively charged binding pocket. The higher frequency is attributed to a conformation with less favorable H-bonding interactions between Y(CD1) and the bound CO. In agreement, mutation of both Y(CD1) and W(G8) to Phe caused the Fe−CO stretching frequency to shift-down to 497 cm^{-1}. These data are consistent with our

earlier studies (*1*, *2*) and indicate that in *Mt*-trHbO Y(CD1) and W(G8) are the residues that interact with the bound CO.

Interactions of Y(CD1) and W(G8) with the Bound O_2. The Fe−O_2 stretching mode of *Mt*-trHbO observed at 559 cm^{-1} is ∼10 cm^{-1} lower than the typical frequency observed for most globins (*23*), where the Fe−O_2 stretching frequency is relatively insensitive to H-bonding to the *distal* oxygen of the heme-bound dioxygen. We have shown previously that hydrogen-bonding to the *proximal* atom of the heme-bound O_2 causes a significant lowering of the Fe−O_2 stretching frequency (*23*, *33*, *34*). The low frequency of this mode in *Mt*-trHbO suggests that the *proximal* oxygen atom of the heme bound O_2 forms an H-bond with a distal residue. This frequency was unaffected in the Y(B10)F mutant but was shifted-down to 556 cm^{-1} in the Y(CD1)F mutant. To explain these results we had proposed that in *Mt*-trHbO Y(B10) and Y(CD1) interact with the *distal* and the *proximal* oxygen atom, respectively, and that in the absence of Y(CD1), Y(B10) would make a strong hydrogen bond to the proximal oxygen. Our present data clearly show that the constraint on the *proximal* oxygen is released significantly when W(G8) is substituted for Phe indicating that W(G8) interacts with the *proximal* oxygen atom. Changing both Y(CD1) and W(G8) for Phe caused no further changes in the Fe−O_2 stretching frequency (564 cm^{-1}) indicating that there is still some constraint on the *proximal* oxygen atom, which may be attributed to the positive edge of the phenyl multipole. Such productive electrostatic interaction has also been described in the myoglobin L(B10)F mutant (*28*−*30*) and in the *Mt*-trHbN Y(B10)F mutant (*18*). In the light of our present observations, the 3 cm^{-1} downshift of ν_{Fe-OO} to 556 cm^{-1} observed previously with the Y(CD1)F mutant may be attributed to the strengthening of the hydrogen bond between W(G8) and the proximal oxygen atom of the heme-bound O_2 caused by a slight repositioning of W(G8) in the absence of the hydrogen bond between W(G8) and Y(CD1).

So far, the enhancement of the ν_{O-O} line has been observed only in the resonance Raman spectra of the oxy derivatives of trHbs from *Chlamydomonas eugametos* (1136 cm^{-1}) (*33*), *Synechocystis* PCC6803 (1133 cm^{-1}) (*33*), *Mt*-trHbO (1140 cm^{-1}) (*23*), and *Campylobacter jejuni* trHb (1132 cm^{-1}) (*35*). It is noteworthy that this mode has not been reported in the resonance Raman spectra of globins with an iron-containing heme coordinated by a proximal histidine. Resonance Raman spectroscopy along with mutagenesis studies indicated that H-bonding with both *proximal* and *distal* oxygen atoms may be required for the enhancement of the O−O stretching mode (*23*, *33*, *35*). The silence of the O−O mode in the resonance Raman spectra of oxy complexes of the two distal pocket mutants Y(CD1)F (*23*) and W(G8)F (data not shown) mutants of *Mt*-trHbO indicates that H-bonding of O−O with Y(CD1) and W(G8) is required for the enhancement of the O−O stretching mode.

O_2 and CO Combination to Mt-trHbO. *Mt*-trHbO combines with O_2, CO, and NO at similar very slow rates (*2*). These slow, ligand-independent combination rates indicate that the electronic factors that give rise to the large ligand-specific differences in most myoglobins and hemoglobins (Hbs) are not dominant in *Mt*-trHbO. Instead these observations are most consistent with limited access of ligands to the heme-iron. Similarly, the comparable slow rate for the reaction of NO with heme-bound O_2 of *Mt*-trHbO demonstrates that access of small molecules to the heme-bound ligands is also limited (*2*).

The crystal structure of cyano-met *Mt*-trHbO provides evidence for a ligand pathway linking the distal cavity to the external solvent space through a path defined by the A(E7)−R(E10) and the porphyrin plane (*1*). Along this pathway two protein bound water molecules (W1 and W2) are found at the entrance of the distal site. W1 is present in all molecules bound to the O atom of carbonyl of A(E7). The second water molecule (W2) is located on the outer side of the heme crevice, next to the heme propionates, and hydrogen bonded to W1. Interestingly, two water molecules are found in essentially the same positions in the distal site of *Tf*-trHbO (*11*). At difference with *Mt*-trHbO W1 in *Tf*-trHbO is hydrogen-bonded to the OH group of Y(B10), which may be attributed to the nature of the bound ligands: acetate in *Tf*-trHbO and cyanide in *Mt*-trHbO. These observations suggest that ligand may enter in *Mt*-trHbO in a way similar to that of myoglobin.

In deoxy myoglobin a noncoordinated water molecule is H-bonded to the Nϵ atom of HisE7 and located very near the heme iron (*36*). Combined mutagenesis and kinetic experiments indicated that the distal water molecule blocks ligand binding and must be displaced for heme ligation to take place (*37*−*41*). The optical and resonance Raman spectra of ferric *Mt*-trHbO are consistent with a water molecule being coordinated to the heme iron (Figure 1) (*23*). Although we do not have direct evidence for the presence of distal water molecule in deoxy *Mt*-trHbO, it is very likely that a water molecule should also be present. It may be noticed here that in the side subunits of the W(G8)F mutant structure a third water molecule (W3) is observed in the inner part of the heme crevice (Figure 7B). W3 is hydrogen bonded to the OH group of the Y(B10) (average distance 2.4 Å), to the cyanide ligand free N atom (average distance 2.7 Å), but also to W1 (average distance 2.6 Å). Thus, W3 may be strategically located for heme coordination, in the absence of the Fe-atom diatomic ligand. Based on the present kinetic data we postulate that in ferrous unliganded *Mt*-trHbO a noncoordinated distal water molecule strongly stabilized by Y(CD1) and W(G8) is located close to the heme iron forming a strong barrier to ligand binding. In addition, the bound water molecules W1 and W2 may also contribute to further blocking access of gaseous ligands to deoxy and oxygenated *Mt*-trHbO.

Role of Distal Y(B10), Y(CD1), and W(G8) in O_2 Stabilization. We have shown previously that replacing Y(B10) and Y(CD1) by Phe causes only small changes in the rate of O_2 dissociation in *Mt*-trHbO (*2*) (Table 2). We now find that mutation of W(G8) increases O_2 dissociation more than 700-fold, indicating that in *Mt*-trHbO the bound O_2 would be mainly stabilized by W(G8). However, O_2 is still relatively strongly bound to the heme iron in the W(G8)F and the Y(CD1)F/W(G8)F mutants, as evidenced by their low rates of O_2 dissociation (Table 2) and their low νFe−O_2 frequencies. In fact, the oxygen dissociation rates of the latter mutants are similar to that reported for *Mt*-trHbN where bound O_2 is strongly stabilized through H-bonding with Y(B10) (Table 2). Analysis of the heme distal site structure indicates that very contained structural variations would be needed for the bound O_2 to be stabilized by the Y(CD1) residue in the W(G8)F mutant, whereas stabilizing effects

related to aromatic−electrostatic interactions linked to the positively charged edge of either Phe residue may also be considered in the Y(CD1)F/W(G8)F mutant. Thus, interpretation of the kinetic data indicates that several H-bonding schemes to the bound O_2 may be operative in mutated *Mt*-trHbO, as supported by our resonance Raman data. Such H-bonding potential implies that ligand escape may always require the simultaneous breaking of several H-bonds, which would explain failure to observe CO geminate recombination (*2*).

Conclusion. W(G8) is an invariant residue in group II and III trHbs, which has no counterpart in other globins. As shown by X-ray diffraction studies (*1*, *10*−*12*, *42*) this residue is sited close to the heme iron atom. Despite this situation, the role of W(G8) in ligand binding has not been investigated so far. The present work thus provides the first direct evidence for a critical role of W(G8) residue in O_2 access and stabilization.

ACKNOWLEDGMENT

We are grateful to Dr. Joel M. Friedman, Dr. Beatrice A. Wittenberg, Dr. Jonathan B. Wittenberg, and Dr. Yannick Ouellet for insightful discussions.

REFERENCES

1. Milani, M., Savard, P. Y., Ouellet, H., Ascenzi, P., Guertin, M., and Bolognesi, M. (2003) A TyrCD1/TrpG8 hydrogen bond network and a TyrB10/TyrCD1 covalent link shape the heme distal site of *Mycobacterium tuberculosis* hemoglobin O, *Proc. Natl. Acad. Sci. U.S.A. 100*, 5766−5771.
2. Ouellet, H., Juszczak, L., Dantsker, D., Samuni, U., Ouellet, Y. H., Savard, P. Y., Wittenberg, J. B., Wittenberg, B. A., Friedman, J. M., and Guertin, M. (2003) Reactions of *Mycobacterium tuberculosis* truncated hemoglobin O with ligands reveal a novel ligand-inclusive hydrogen bond network, *Biochemistry 42*, 5764−5774.
3. Ouellet, H., Ouellet, Y., Richard, C., Labarre, M., Wittenberg, B., Wittenberg, J., and Guertin, M. (2002) Truncated hemoglobin HbN protects *Mycobacterium bovis* from nitric oxide, *Proc. Natl. Acad. Sci. U.S.A. 99*, 5902−5907.
4. Herold, S., Exner, M., and Nauser, T. (2001) Kinetic and mechanistic studies of the NO*-mediated oxidation of oxymyoglobin and oxyhemoglobin, *Biochemistry 40*, 3385−3395.
5. Eich, R. F., Li, T., Lemon, D. D., Doherty, D. H., Curry, S. R., Aitken, J. F., Mathews, A. J., Johnson, K. A., Smith, R. D., Phillips, G. N., Jr., and Olson, J. S. (1996) Mechanism of NO-induced oxidation of myoglobin and hemoglobin, *Biochemistry 35*, 6976−6983.
6. Ouellet, H., Ranguelova, K., Labarre, M., Wittenberg, J. B., Wittenberg, B. A., Magliozzo, R. S., and Guertin, M. (2007) Reaction of *Mycobacterium tuberculosis* truncated hemoglobin O with hydrogen peroxide: evidence for peroxidatic activity and formation of protein-based radicals, *J. Biol. Chem. 282*, 7491−7503.
7. Vuletich, D. A., and Lecomte, J. T. (2006) A phylogenetic and structural analysis of truncated hemoglobins, *J. Mol. Evol. 62*, 196−210.
8. Vinogradov, S. N., Hoogewijs, D., Bailly, X., Arredondo-Peter, R., Guertin, M., Gough, J., Dewilde, S., Moens, L., and Vanfleteren, J. R. (2005) Three globin lineages belonging to two structural classes in genomes from the three kingdoms of life, *Proc. Natl. Acad. Sci. U.S.A. 102*, 11385−11389.
9. Wittenberg, J. B., Bolognesi, M., Wittenberg, B. A., and Guertin, M. (2002) Truncated hemoglobins: a new family of hemoglobins widely distributed in bacteria, unicellular eukaryotes, and plants, *J. Biol. Chem. 277*, 871−874.
10. Giangiacomo, L., Ilari, A., Boffi, A., Morea, V., and Chiancone, E. (2005) The truncated oxygen-avid hemoglobin from *Bacillus subtilis*: X-ray structure and ligand binding properties, *J. Biol. Chem. 280*, 9192−9202.
11. Bonamore, A., Ilari, A., Giangiacomo, L., Bellelli, A., Morea, V., and Boffi, A. (2005) A novel thermostable hemoglobin from the actinobacterium *Thermobifida fusca*, *FEBS J. 272*, 4189−4201.
12. Ilari, A., Kjelgaard, P., von Wachenfeldt, C., Catacchio, B., Chiancone, E., and Boffi, A. (2007) Crystal structure and ligand binding properties of the truncated hemoglobin from *Geobacillus stearothermophilus*, *Arch. Biochem. Biophys. 457*, 85−94.
13. Watts, R. A., Hunt, P. W., Hvitved, A. N., Hargrove, M. S., Peacock, W. J., and Dennis, E. S. (2001) A hemoglobin from plants homologous to truncated hemoglobins of microorganisms, *Proc. Natl. Acad. Sci. U.S.A. 98*, 10119−10124.
14. Bolognesi, M., Bordo, D., Rizzi, M., Tarricone, C., and Ascenzi, P. (1997) Nonvertebrate hemoglobins: structural bases for reactivity, *Prog. Biophys. Mol. Biol. 68*, 29−68.
15. Milani, M., Pesce, A., Ouellet, Y., Dewilde, S., Friedman, J., Ascenzi, P., Guertin, M., and Bolognesi, M. (2004) Heme-ligand tunneling in group I truncated hemoglobins, *J. Biol. Chem. 279*, 21520−21525.
16. Milani, M., Pesce, A., Ouellet, Y., Ascenzi, P., Guertin, M., and Bolognesi, M. (2001) *Mycobacterium tuberculosis* hemoglobin N displays a protein tunnel suited for O_2 diffusion to the heme, *EMBO J. 20*, 3902−3909.
17. Hargrove, M. S., and Olson, J. S. (1996) The stability of holomyoglobin is determined by heme affinity, *Biochemistry 35*, 11310−11318.
18. Ouellet, Y., Milani, M., Couture, M., Bolognesi, M., and Guertin, M. (2006) Ligand interactions in the distal heme pocket of *Mycobacterium tuberculosis* truncated hemoglobin N: roles of TyrB10 and GlnE11 residues, *Biochemistry 45*, 8770−8781.
19. (1994) Collaborative Computational Project, Number 4 (CCP4). The CCP4 suite. Programs for protein crystallography, *Acta Crystallogr., Sect. D: Biol. Crystallogr. 50*, 760−763.
20. Steller, I., Bolotovsky, R., and Rossmann, M. (1997) An Algorithm for Automatic Indexing of Oscillation Images using Fourier Analysis, *J. Appl. Crystallogr. 30*, 1036−1040.
21. Murshudov, G. N., Vagin, A. A., and Dodson, E. J. (1997) Refinement of macromolecular structures by the maximum-likelihood method, *Acta Crystallogr., Sect. D: Biol. Crystallogr. 53*, 240−255.
22. Berman, H. M., Westbrook, J., Feng, Z., Gilliland, G., Bhat, T. N., Weissig, H., Shindyalov, I. N., and Bourne, P. E. (2000) The Protein Data Bank, *Nucleic Acids Res. 28*, 235−242.
23. Mukai, M., Savard, P. Y., Ouellet, H., Guertin, M., and Yeh, S. R. (2002) Unique ligand-protein interactions in a new truncated hemoglobin from *Mycobacterium tuberculosis*, *Biochemistry 41*, 3897−3905.
24. Spiro, T. G., and Li, X. Y. (1988) Resonance Raman spectroscopy of metalloporphyrins, in *Biological Applications of Raman Spectroscopy*, John Wiley & Sons, New York.
25. Wang, J., Caughey, W. S., and Rousseau, D. L. (1996) Resonance Raman scattering: A probe of heme protein-bound nitric oxide, *Methods Nitric Oxide Res.*, 427−454.
26. Spiro, T. G., and Wasbotten, I. H. (2005) CO as a vibrational probe of heme protein active sites, *J. Inorg. Biochem. 99*, 34−44.
27. Pesce, A., Nardini, M., Ascenzi, P., Geuens, E., Dewilde, S., Moens, L., Bolognesi, M., Riggs, A. F., Hale, A., Deng, P., Nienhaus, G. U., Olson, J. S., and Nienhaus, K. (2004) Thr-E11 regulates O2 affinity in *Cerebratulus lacteus* mini-hemoglobin, *J. Biol. Chem. 279*, 33662−33672.
28. Hirota, S., Li, T., Phillips, G. N., Jr., Olson, J. S., Mukai, M., and Kitagawa, T. (1996) Perturbation of the $Fe-O_2$ bond by nearby residues in heme pocket: Observation of ν_{Fe-O_2} Raman bands for oxymyoglobin mutants, *J. Am. Chem. Soc. 118*, 7845−7846.
29. Springer, B. A., Sligar, S. G., Olson, J. S., and Phillips, G. N., Jr. (1994) Mechanisms of ligand recognition in myoglobin, *Chem. Rev. 94*, 699−714.
30. Zhao, X., Vyas, K., Nguyen, B. D., Rajarathnam, K., La Mar, G. N., Li, T., Phillips, G. N., Jr., Eich, R. F., Olson, J. S., Ling, J., and Bocian, D. F. (1995) A double mutant of sperm whale myoglobin mimics the structure and function of elephant myoglobin, *J. Biol. Chem. 270*, 20763−20774.
31. Crumpton, M. J., and Polson, A. (1965) A comparison of the conformation of sperm whale metmyoglobin with that of apomyoglobin, *J. Mol. Biol. 11*, 722−729.
32. Kawahara, K., Kirshner, A. G., and Tanford, C. (1965) Dissociation of human CO-hemoglobin by urea, guanidine hydrochloride, and other reagents, *Biochemistry 4*, 1203−1213.

33. Das, T. K., Couture, M., Ouellet, Y., Guertin, M., and Rousseau, D. L. (2001) Simultaneous observation of the O−O and Fe−O_2 stretching modes in oxyhemoglobins, *Proc. Natl. Acad. Sci. U.S.A. 98*, 479−484.
34. Yeh, S. R., Couture, M., Ouellet, Y., Guertin, M., and Rousseau, D. L. (2000) A cooperative oxygen binding hemoglobin from *Mycobacterium tuberculosis*. Stabilization of heme ligands by a distal tyrosine residue, *J. Biol. Chem. 275*, 1679−1684.
35. Lu, C., Egawa, T., Wainwright, L. M., Poole, R. K., and Yeh, S. R. (2007) Structural and functional properties of a truncated hemoglobin from a food-borne pathogen *Campylobacter jejuni*, *J. Biol. Chem.*, submitted.
36. Vojtechovsky, J., Chu, K., Berendzen, J., Sweet, R. M., and Schlichting, I. (1999) Crystal structures of myoglobin-ligand complexes at near-atomic resolution, *Biophys. J. 77*, 2153−2174.
37. Rohlfs, R. J., Mathews, A. J., Carver, T. E., Olson, J. S., Springer, B. A., Egeberg, K. D., and Sligar, S. G. (1990) The effects of amino acid substitution at position E7 (residue 64) on the kinetics of ligand binding to sperm whale myoglobin, *J. Biol. Chem. 265*, 3168−3176.
38. Olson, J. S., and Phillips, G. N., Jr. (1996) Kinetic pathways and barriers for ligand binding to myoglobin, *J. Biol. Chem. 271*, 17596.
39. Olson, J. S., and Phillips, G. N., Jr. (1997) Myoglobin discriminates between O_2, NO and CO by electrostatic interactions with the bound ligands, *J. Biol. Inorg. Chem. 2*, 544−552.
40. Scott, E. E., Gibson, Q. H., and Olson, J. S. (2001) Mapping the pathways for O_2 entry into and exit from myoglobin, *J. Biol. Chem. 276*, 5177−5188.
41. Goldbeck, R. A., Bhaskaran, S., Ortega, C., Mendoza, J. L., Olson, J. S., Soman, J., Kliger, D. S., and Esquerra, R. M. (2006) Water and ligand entry in myoglobin: assessing the speed and extent of heme pocket hydration after CO photodissociation, *Proc. Natl. Acad. Sci. U.S.A. 103*, 1254−1259.
42. Nardini, M., Pesce, A., Labarre, M., Richard, C., Bolli, A., Ascenzi, P., Guertin, M., and Bolognesi, M. (2006) Structural determinants in the group III truncated hemoglobin from *Campylobacter jejuni*, *J. Biol. Chem. 281*, 37803−37812.
43. Couture, M., Das, T. K., Lee, H. C., Peisach, J., Rousseau, D. L., Wittenberg, B. A., Wittenberg, J. B., and Guertin, M. (1999) *Chlamydomonas* chloroplast ferrous hemoglobin. Heme pocket structure and reactions with ligands, *J. Biol. Chem. 274*, 6898−6910.
44. Couture, M., Das, T. K., Savard, P. Y., Ouellet, Y., Wittenberg, J. B., Wittenberg, B. A., Rousseau, D. L., and Guertin, M. (2000) Structural investigations of the hemoglobin of the cyanobacterium *Synechocystis* PCC6803 reveal a unique distal heme pocket, *Eur. J. Biochem. 267*, 4770−4780.
45. Das, T. K., Weber, R. E., Dewilde, S., Wittenberg, J. B., Wittenberg, B. A., Yamauchi, K., Van Hauwaert, M. L., Moens, L., and Rousseau, D. L. (2000) Ligand binding in the ferric and ferrous states of *Paramecium* hemoglobin, *Biochemistry 39*, 14330−14340.
46. Couture, M., Yeh, S. R., Wittenberg, B. A., Wittenberg, J. B., Ouellet, Y., Rousseau, D. L., and Guertin, M. (1999) A cooperative oxygen-binding hemoglobin from *Mycobacterium tuberculosis*, *Proc. Natl. Acad. Sci. U.S.A. 96*, 11223−11228.
47. Potterton, L., McNicholas, S., Krissinel, E., Gruber, J., Cowtan, K., Emsley, P., Murshudov, G. N., Cohen, S., Perrakis, A., and Noble, M. (2004) Developments in the CCP4 molecular-graphics project, *Acta Crystallogr., Sect. D: Biol. Crystallogr. 60*, 2288−2294.

BI7010288